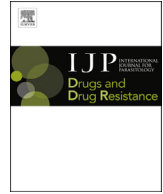




Contents lists available at ScienceDirect

International Journal for Parasitology: Drugs and Drug Resistance

journal homepage: www.elsevier.com/locate/ijppaw

The *Ascaris suum* nicotinic receptor, ACR-16, as a drug target: Four novel negative allosteric modulators from virtual screening



Fudan Zheng^a, Alan P. Robertson^b, Melanie Abongwa^b, Edward W. Yu^{a, c},
Richard J. Martin^{b, *}

^a Department of Chemistry, College of Liberal Arts and Sciences, Iowa State University, Ames, IA 50011, USA

^b Department of Biomedical Sciences, College of Veterinary Medicine, Iowa State University, Ames, IA 50011, USA

^c Department of Physics and Astronomy, College of Liberal Arts and Sciences, Iowa State University, Ames, IA 50011, USA

ARTICLE INFO

Article history:

Received 6 November 2015

Received in revised form

28 January 2016

Accepted 5 February 2016

Available online 10 February 2016

Keywords:

Asu-ACR-16

Structure-based drug discovery

Homology modeling

Orthosteric site

Allosteric modulator

Xenopus expression

ABSTRACT

Soil-transmitted helminth infections in humans and livestock cause significant debility, reduced productivity and economic losses globally. There are a limited number of effective anthelmintic drugs available for treating helminths infections, and their frequent use has led to the development of resistance in many parasite species. There is an urgent need for novel therapeutic drugs for treating these parasites. We have chosen the ACR-16 nicotinic acetylcholine receptor of *Ascaris suum* (Asu-ACR-16), as a drug target and have developed three-dimensional models of this transmembrane protein receptor to facilitate the search for new bioactive compounds. Using the human $\alpha 7$ nAChR chimeras and *Torpedo marmorata* nAChR for homology modeling, we defined orthosteric and allosteric binding sites on the Asu-ACR-16 receptor for virtual screening. We identified four ligands that bind to sites on Asu-ACR-16 and tested their activity using electrophysiological recording from Asu-ACR-16 receptors expressed in *Xenopus* oocytes. The four ligands were acetylcholine inhibitors (SB-277011-A, IC₅₀, 3.12 ± 1.29 μM; (+)-butaclamol Cl, IC₅₀, 9.85 ± 2.37 μM; fmoc-1, IC₅₀, 10.00 ± 1.38 μM; fmoc-2, IC₅₀, 16.67 ± 1.95 μM) that behaved like negative allosteric modulators. Our work illustrates a structure-based in silico screening method for seeking anthelmintic hits, which can then be tested electrophysiologically for further characterization.

© 2016 The Authors. Published by Elsevier Ltd on behalf of Australian Society for Parasitology. This is an open access article under the CC BY license (<http://creativecommons.org/licenses/by/4.0/>).

1. Introduction

Soil-transmitted gastrointestinal nematodes, namely roundworms, whipworms and hookworms, infect approximately two billion people worldwide and pose a significant health challenge to humans and animals (de Silva et al., 2003; Bethony et al., 2006). The infections with the soil-transmitted helminths can cause malnutrition, iron-deficiency anemia and impaired cognitive performance (Crompton, 2000; Hotez et al., 2007). Currently, there are no effective vaccines available (Hewitson and Maizels, 2014), and sanitation is not adequate in many countries. The World Health Organization (WHO) recommends four anthelmintics for treatment and prophylaxis of soil-transmitted nematode infections:

Abbreviations: ECD, extracellular domain; TID, transmembrane and intracellular domain; (+), principal subunit; (–), complementary subunit; NAM, negative allosteric modulator; nAChR, nicotinic acetylcholine receptor; AChBP, acetylcholine-binding protein.

* Corresponding author. 2018 Vet Med, Ames, IA 50011-1250, USA.

E-mail address: rjmartin@iastate.edu (R.J. Martin).

albendazole, mebendazole, levamisole and pyrantel (Keiser and Utzinger, 2008). The repeated use of a limited number of anthelmintic drugs has led to an increase in drug resistance in animals and there are similar concerns for humans. It is therefore important to identify novel therapeutic compounds that selectively target receptors of parasitic nematodes so that we maintain effective therapeutics.

The nicotinic acetylcholine receptors (nAChRs) are pentameric ligand-gated ion channels that mediate synaptic transmission at neuromuscular junctions of vertebrates and invertebrates (Changeux and Edelstein, 1998). The neurotransmitter, acetylcholine, activates nAChRs by binding to orthosteric binding sites on the extracellular domain of the receptor and triggers the opening of the channel pore in the transmembrane domain. The opening of the nicotinic receptors leads to an influx of sodium and calcium depending on the receptor subtypes, as well as an output of potassium ions, followed by membrane depolarization and muscle contraction.

Nicotinic anthelmintics are selective agonists of nematode

muscle nAChRs which cause spastic paralysis of the parasites (Martin and Robertson, 2010; Buxton et al., 2014). There are three different pharmacological subtypes of nAChRs present on muscle of *Ascaris suum*. The anthelmintics, levamisole and pyrantel are selective agonists of L-subtypes of nAChRs in *A. suum* (Martin et al., 2012). Bephenium selectively activates B-subtypes of nAChRs. Nicotine and oxantel selectively activate N-subtypes of nAChRs in *A. suum* (Qian et al., 2006). The anthelmintic monopantel activates nAChRs which are composed of DEG-3-like subunits (*Haemonchus contortus* MPTL-1, *Caenorhabditis elegans* ACR-20 and *H. contortus* ACR-23 subunits (Rufener et al., 2010; Buxton et al., 2014). We have selected the N-subtype of nAChR that is composed of ACR-16 subunits (Ballivet et al., 1996; Polli et al., 2015) for a drug target, because it is pharmacologically different to the other nicotinic receptor subtypes (Raymond et al., 2000), for further study. Asu-ACR-16 transcript has been found in *A. suum* muscle and may be involved in locomotion.

The ACR-16 nicotinic acetylcholine receptor of *A. suum* (Asu-ACR-16) is a homomeric receptor made up of five identical α subunits. Homomeric nAChRs have five identical orthosteric binding sites where agonists and competitive antagonists bind at the interface of two adjacent subunits. The orthosteric site is in the extracellular domain and is formed by the loops A, B & C of the principal subunit and by the loops D, E & F of the complementary subunit (Galzi et al., 1991; Arias, 2000). In addition, three allosteric binding sites close to the orthosteric binding sites in the extracellular domain have been observed in the $\alpha 7$ nAChR-AChBP chimera (Spurny et al., 2015). In the transmembrane domain, an intrasubunit allosteric binding site has been found in *Rattus norvegicus* $\alpha 7$ nAChR (Young et al., 2008), while an intersubunit allosteric binding site has been found in *C. elegans* glutamate-gated chloride channel (GluCl) (Hibbs and Gouaux, 2011). These well-studied binding sites in nAChRs or other Cys-loop receptors provided our framework for characterizing putative orthosteric and allosteric sites in Asu-ACR-16.

Because of the lack of a crystal structure for Asu-ACR-16, we used homology modeling to predict the protein structure, based on the observations that proteins with similar sequences usually have similar structures (Cavasotto and Phatak, 2009). In this study, we used homology modeling to predict the three-dimensional structure of Asu-ACR-16, based on the observed experimental structures of the human $\alpha 7$ nAChR chimeras and the *Torpedo marmorata* nAChR as templates. Virtual screening was performed for the ACR-16 orthosteric binding sites, using the predicted structure to identify the potential candidates of agonists and competitive antagonists. Allosteric binding sites were also used to examine the binding properties of the virtual screening hits. Subsequently, we tested the pharmacological profiles of virtual screening hits on Asu-ACR-16 receptors expressed in *Xenopus laevis* oocytes, using a two-electrode voltage clamp to test the activity of the hits on the receptors.

2. Materials and methods

2.1. Identification of template structures

We selected the extracellular domain of Asu-ACR-16 (ECD-Asu-ACR-16) because it forms a homologue that allows homology modeling. In addition, many of the agonists that activate Asu-ACR-16, acetylcholine, nicotine, cytosine, epibatidine (Abongwa et al., 2016), are also known to bind to the orthosteric binding sites of extracellular domain of *Lymnaea stagnalis* AChBP or *A. californica* AChBP (Celie et al., 2004; Li et al., 2011; Rucktooa et al., 2012; Olsen et al., 2014a). In addition to the orthosteric binding site, three separate allosteric binding sites in the extracellular domain of $\alpha 7$

nAChR are now recognized (Bertrand et al., 2008; Pan et al., 2012; Spurny et al., 2015), increasing the possibility of identifying allosteric modulators.

The amino acid sequence of Asu-ACR-16 (Fig. 1) was obtained from the UniProtKB/SwissProt database with the accession number F1KYJ9 (Wang et al., 2011). Structural templates were identified by using BLASTP on NCBI network service (Altschul et al., 1997) and PSI-BLAST on the ProtMod server (Rychlewski et al., 2000) by searching in the Protein Data Bank (Berman et al., 2000). Three crystal structures of human $\alpha 7$ nAChR chimeras with different co-crystal ligands in orthosteric binding site were used: epibatidine bound (PDB code: 3SQ6; Li et al., 2011), no ligand (PDB code: 3SQ9; Li et al., 2011), and α -bungarotoxin bound (PDB code: 4HQP; Huang et al., 2013). These structures were selected as the templates for three different bound-forms of the ECD-Asu-ACR-16. The three models were: the agonist-bound form ECD-Asu-ACR-16; the apo form ECD-Asu-ACR-16 and; the antagonist-bound form ECD-Asu-ACR-16 (Fig. 2A).

We modeled the transmembrane and intracellular domains of Asu-ACR-16 (TID-Asu-ACR-16, Fig. 2B) because of the presence of an intrasubunit allosteric binding site that is found in $\alpha 7$ nAChR and an intersubunit allosteric binding site that is demonstrated in a Cys-loop receptor, GluCl crystal structure in complex with ivermectin (Young et al., 2008; Bertrand et al., 2008; Hibbs and Gouaux, 2011). Ivermectin is a known allosteric modulator of $\alpha 7$ nAChRs (Krause et al., 1998). The *T. marmorata* nAChR (PDB code: 2BG9 chain A; Unwin, 2005) is the only pentameric nAChR structure with the transmembrane domains and partial intracellular domains determined. Therefore, the transmembrane and intracellular domains of *T. marmorata* nAChR (TID-Tma-nAChR) were selected as the template for our TID-Asu-ACR-16 model.

The sequence of the ECD-Asu-ACR-16 and the human $\alpha 7$ nAChR chimera (SwissProt ID: P36544; Peng et al., 1994) were aligned using CLUSTALW multiple alignment (Thompson et al., 1994). The sequence of the TID-Asu-ACR-16 and TID-Tma-nAChR (SwissProt ID: P02711; Devillers-Thierry et al., 1983, 1984) were aligned using CLUSTALW.

2.2. Homology modeling of Asu-ACR-16

We used Modeller (Eswar et al., 2007) to build a three-dimensional model of ECD-Asu-ACR-16 and used JACKAL (http://wiki.c2b2.columbia.edu/honiglab_public/index.php/Software:Jackal) to build the model of TID-Asu-ACR-16 for each of the five subunits. These five subunits were then assembled to generate the pentamer using COOT software (Emsley and Cowtan, 2004). The model geometry was first refined manually, and then optimized by PHENIX software (Adams et al., 2010). Each of the TID-Asu-ACR-16 subunits were then merged into the ECD-Asu-ACR-16 model by using COOT to edit and alter the C_{α} coordinates of residues around the outer membrane regions. The final optimized pentameric model was then visualized using the program PyMol (The PyMOL Molecular Graphics System, Version 1.7.4, Schrödinger, and LLC., Figs. 2C & S1).

2.3. Structure-based virtual screening

Smiles strings of ligands were downloaded from the lead-like subset of commercially available compounds in the ZINC Database (Irwin et al., 2012) and were converted initially to PDB formats using the PHENIX-eLBOW program (Moriarty et al., 2009). The ligand and receptor input files were then prepared in PDBQT format for AutoDock Vina by using the AutoDock Tools package (Morris et al., 2009). For initial screening, a docking area was defined visually around the orthosteric binding site of ECD-Asu-ACR-16

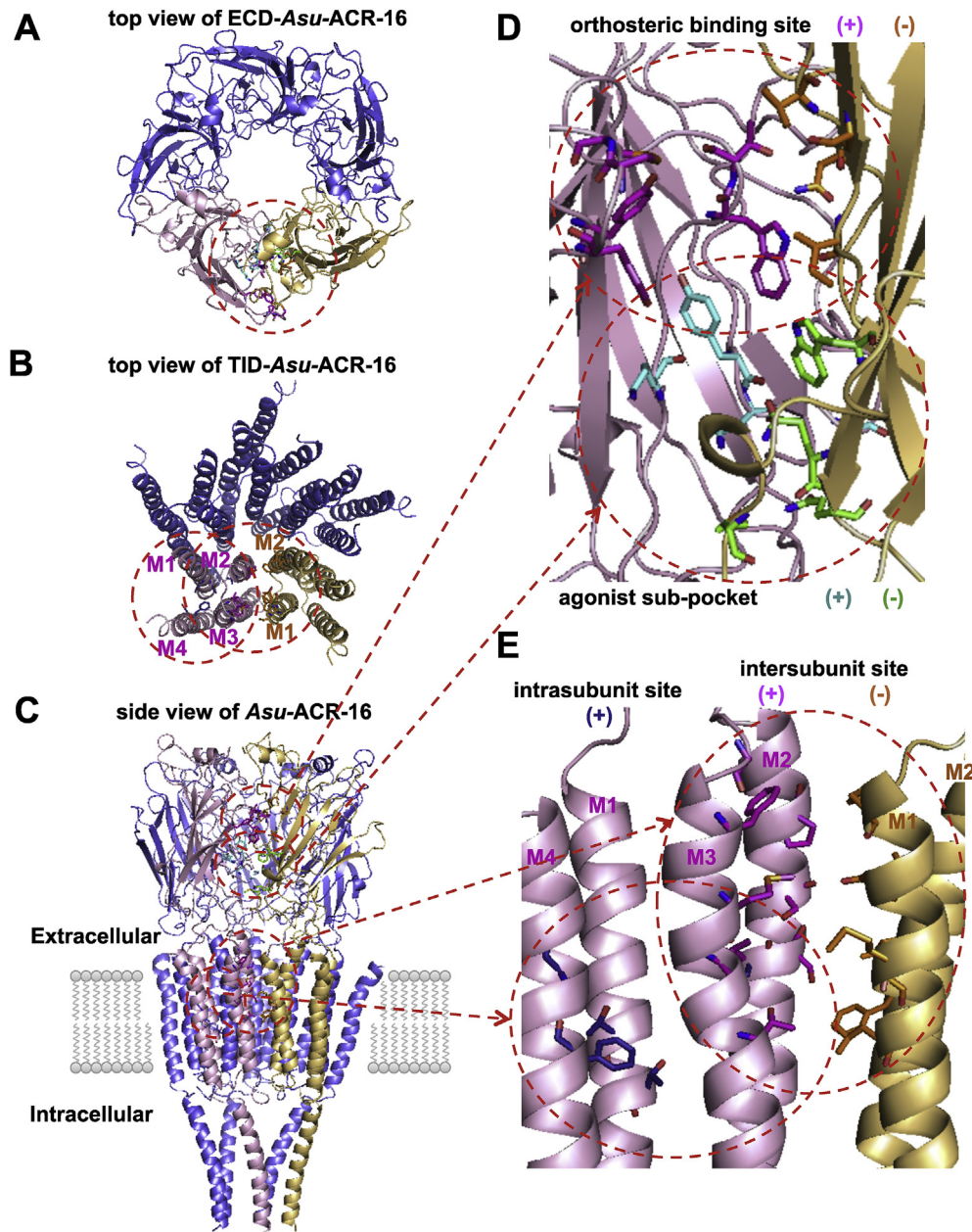
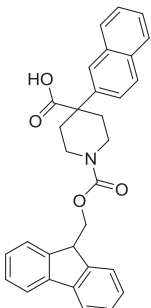
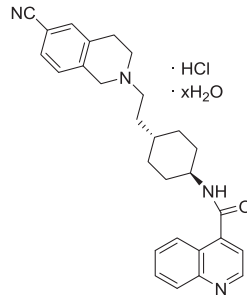
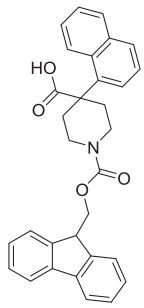
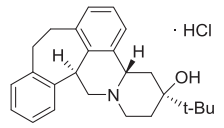


Fig. 2. (A) Ribbon diagram of the antagonist-bound model of ECD-Asu-ACR-16 viewed from the synaptic cleft, showing the location of the orthosteric binding site and agonist sub-pocket. For clarity, only the front two subunits are highlighted (principal subunit, light pink; complementary subunit, yellow). The residues that contribute to the orthosteric binding site (principal side, pink; complementary side, orange) and the agonist sub-pocket (principal side, turquoise; complementary side, green) are represented by sticks and highlighted inside the red dotted circle. (B) Ribbon diagram of the antagonist-bound model of TID-Asu-ACR-16 viewed above the membrane, showing the location of two transmembrane allosteric binding sites. For clarity, only the front two subunits are highlighted (principal subunit, light pink; complementary subunit, yellow). The residues that contribute to the intersubunit site (principal side, pink; complementary side, orange) and intrasubunit site (principal side, purpleblue) are represented by sticks and highlighted inside the red dotted circle. (C) Ribbon diagram of the antagonist-bound model of full-length Asu-ACR-16 viewed parallel to the membrane plane, showing the location of the orthosteric binding site and the agonist sub-pocket in the extracellular domain, the intersubunit and intrasubunit binding sites in the transmembrane domain. For clarity, only the front two subunits are highlighted (principal subunit, light pink; complementary subunit, yellow). The residues that contribute to the ligand binding sites are represented by sticks (orthosteric site: (+), pink; (-), orange; agonist sub-pocket: (+), turquoise; (-), green; intersubunit transmembrane site: (+), pink; (-), orange; intrasubunit transmembrane site: purpleblue) and highlighted inside the red dotted circle. (D) Detailed view of the orthosteric binding site and agonist sub-pocket in the antagonist-bound model of ECD-Asu-ACR-16. The principal subunit is colored light pink, whereas the complementary subunit is colored yellow. The residues that contribute to the orthosteric binding site (principal side, pink; complementary side, orange) and the agonist sub-pocket (principal side, turquoise; complementary side, green) are represented by sticks and highlighted inside the red dotted circle. Carbon is in either turquoise or green. Nitrogen is in blue. Oxygen is in red. (E) Detailed view of the transmembrane allosteric binding sites in the antagonist-bound model of TID-Asu-ACR-16. The principal subunit is colored light pink, whereas the complementary subunit is colored yellow. The residues that contribute to intersubunit site (principal side, pink; complementary side, orange) and intrasubunit site (principal side, purpleblue) are represented by sticks and highlighted inside the red dotted circle. Carbon is in either pink or orange or purpleblue. Nitrogen is in blue. Oxygen is in red. Sulfur is in yellow. (For interpretation of the references to colour in this figure legend, the reader is referred to the web version of this article.)

ligands (44%) were also specifically docked into five allosteric binding pockets: the agonist sub-pocket (Fig. S2C & S2D); the

vestibule pocket (Fig. S2E & S2F); the top pocket (Fig. S2G & S2H); the intersubunit and; the intrasubunit transmembrane sites (Fig. 2E

Table 1
Physicochemical properties and chemical structures of four virtual screen hits. The four hits are: fmoc-4-(naphthalen-2-yl)-piperidine-4-carboxylic acid (fmoc-2), SB-277011-A hydrochloride hydrate (SB-277011-A), fmoc-4-(naphthalen-1-yl)-piperidine-4-carboxylic acid (fmoc-1), (+)-butaclamol hydrochloride ((+)-butaclamol Cl). The molecular mass (Mol. Mass), number of hydrogen bond donors, number of hydrogen bond acceptors, number of rotatable bonds and partition coefficient (xlogP) are listed for each hits.

ZINC ID	44122512	26574567	44122502	02008410
Hits	fmoc-2	SB-277011-A	fmoc-1	(+)-butaclamol Cl
Structure				
Mol. Mass	478	475	478	363
H-bond donors	0	1	0	2
H-bond acceptors	5	5	5	2
Rotatable bonds	5	5	5	1
XlogP	6.04	4.27	6.02	4.96

S2I S2J). The docking area was defined visually around each allosteric binding pockets of Asu-ACR-16 by a grid box of $40 \text{ \AA} \times 40 \text{ \AA} \times 40 \text{ \AA}$ using 0.375 \AA grid point spacing in AutoGrid. The docking was performed by AutoDock Vina (Fig. 3).

2.4. In vitro synthesis of crRNA and microinjection into *Xenopus laevis* oocytes

We used TRIzol (Invitrogen™) to extract the total RNA samples from a 1 cm muscle flap and dissected the whole pharynx of *A. suum*. The first-strand of cDNA was synthesized with oligo RACER primer, Random Hexamer and superscript III reverse transcriptase (Invitrogen, Carlsbad, CA, USA) from total RNA in the muscle and pharynx by reverse transcription polymerase chain reaction (RT-PCR). Full-length Asu-acr-16 cDNA was amplified with the forward primer TTGATGTAGTGGCGTCTGT, ATCACGCATTACGGTTGATG and the reverse primer GCATTGATGTTCCCTCACCT, ATTAGCGTCCCAAGTGGTTG (Boulin et al., 2011). The XhoI and ApaI restriction enzymes were used to digest the amplified product, which was then cloned into pTB207 expression vector (Boulin et al., 2008) and linearized by NheI. We used the mMessage mMachine T7 kit (Ambion) to in vitro transcribe the linearized cDNA to crRNA, which was then precipitated with lithium chloride, re-suspended in RNase-free water, aliquoted and stored at $-80 \text{ }^\circ\text{C}$.

The ancillary protein RIC-3 is required for the expression of ACR-16 in *Xenopus* oocytes (Halevi et al., 2003). A 50 nL crRNA mixture was prepared with 25 ng Asu-acr-16 crRNA, 5 ng Asu-ric-3 crRNA (SwissProt ID: F1L1D9; Wang et al., 2011) dissolved in RNase-free water. The nanoject II microinjector (Drummond Scientific, PA, USA) was used to inject the crRNA mixture into the animal pole of the de-folliculated *X. laevis* oocyte (Ecocyte Bioscience, Austin, TX, USA).

The injected oocytes were separated into 96-well culture plates and incubated in the incubation solution (pH 7.5), which is composed of 100 mM NaCl, 2 mM KCl, 1.8 mM $\text{CaCl}_2 \cdot 2\text{H}_2\text{O}$, 1 mM $\text{MgCl}_2 \cdot 6\text{H}_2\text{O}$, 5 mM HEPES, 2.5 mM Na pyruvate, 100 U/mL penicillin, 100 $\mu\text{g}/\text{mL}$ streptomycin and changed daily. The injected oocytes were stored at $19 \text{ }^\circ\text{C}$ for 4–8 days to allow the receptor to be expressed.

2.5. Two-electrode voltage-clamp oocyte recording

We used two-electrode voltage-clamp electrophysiology to record the inward current generated by the activated Asu-ACR-16 receptors expressed in *X. laevis* oocytes. 100 μM BAPTA-AM (final concentration) was added into the oocyte incubation solution 4 h prior to recording, to prevent the current produced by the endogenous calcium-activated chloride channels during recording. An Axoclamp 2B amplifier (Molecular Devices, CA, USA) was used for recording and oocytes were held at -60 mV . A PC computer with software Clampex 9.2 (Molecular Devices, CA, USA) was used to acquire the recording data. The microelectrodes used to measure current in oocytes were pulled on a Flaming/Brown horizontal electrode puller (Model P-97, Sutter Instruments), filled with 3M KCl and had resistances of 20–30 M Ω . The microelectrode tips were broken back carefully with Kimwipes (Wilmington, NC, USA) to reduce the resistance to 2–5 M Ω . The recording solution was: 100 mM NaCl, 2.5 mM KCl, 1 mM $\text{CaCl}_2 \cdot 2\text{H}_2\text{O}$ and 5 mM HEPES, pH 7.3 (Buxton et al., 2014). Oocytes were placed into a tiny groove of the narrow oocyte recording chamber. The Digidata 1322A (Molecular Devices, CA, USA) was used to control the switches that controlled the perfusion of the chamber at a speed of 4–6 ml/min.

100 μM acetylcholine was applied initially for 10 s as a control to check the viability of the oocytes and Asu-ACR-16 expression for all the recordings. Recording solution was then used to wash out the drug from the oocytes for 2–3 min before next application of drug perfusion.

2.6. Drugs

Table 1 lists the compounds used, their chemical properties and structures. Fmoc-4-(naphthalen-2-yl)-piperidine-4-carboxylic acid (fmoc-2), SB-277011-A hydrochloride hydrate (SB-277011-A), fmoc-4-(naphthalen-1-yl)-piperidine-4-carboxylic acid (fmoc-1) and (+)-butaclamol hydrochloride ((+)-butaclamol Cl), acetylcholine chloride (ach), methyllycaconitine citrate salt (mla) were purchased from Sigma–Aldrich (St Louis, MO, USA). Levamisole hydrochloride (levamisole) was purchased from MP Biomedicals (Santa Ana, CA, USA). With the exception of ach and mla which were dissolved in the recording solution, the rest of chemicals were dissolved in dimethyl sulfoxide (DMSO) to make stock solutions. Stock solutions of 100 mM

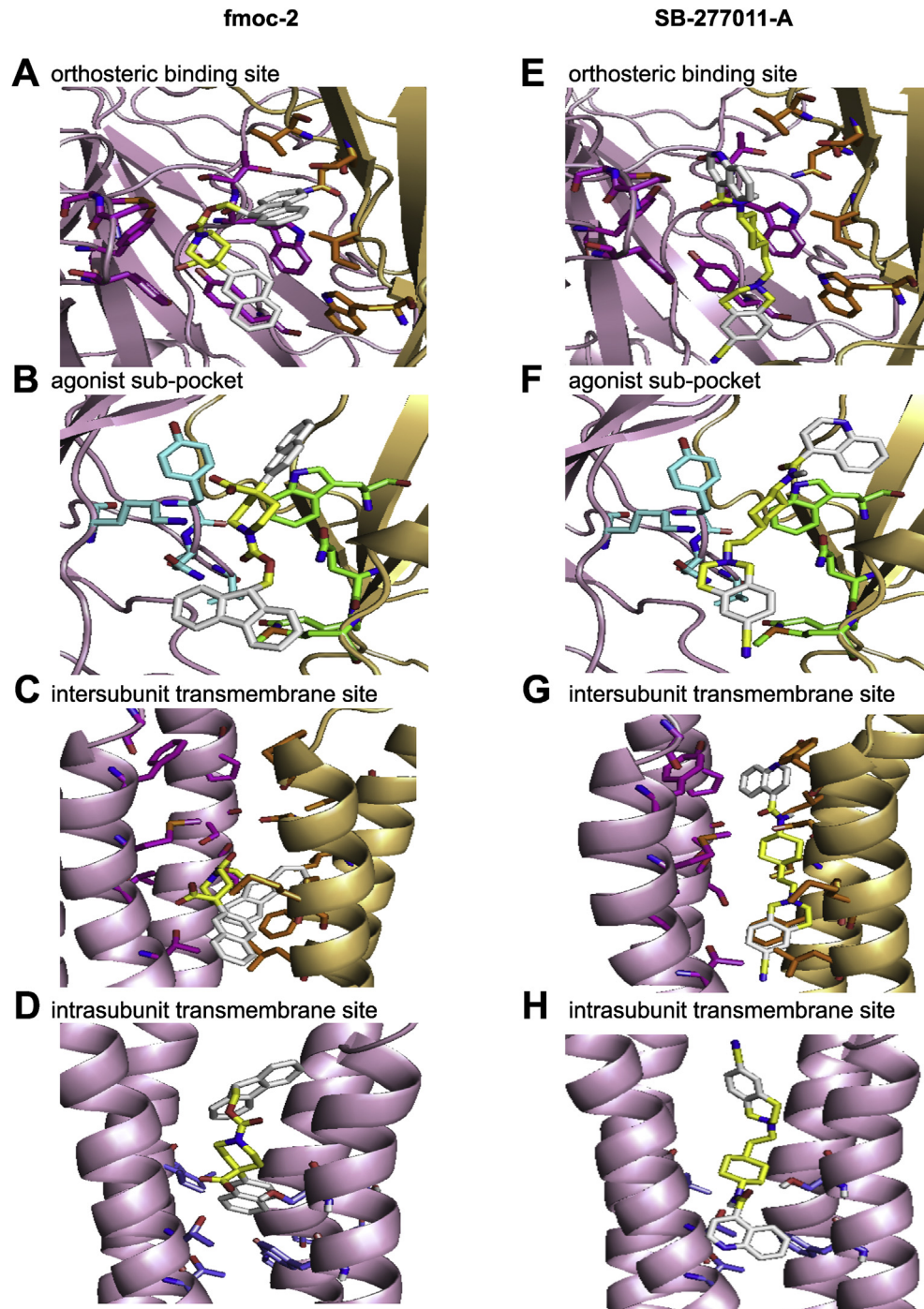


Fig. 3. Binding modes of four virtual screening hits in the orthosteric binding site, the agonist sub-pocket, the intersubunit and intrasubunit transmembrane allosteric binding pockets of the antagonist-bound model of Asu-ACR-16: (A), (B), (C), (D) fmc-2; (E), (F), (G), (H) SB-277011-A; (I), (J), (K) fmc-1; (L), (M), (N), (O) (+)-butaclamol Cl. Hits docked into the binding pockets are represented by sticks (carbon in yellow; ring in white; nitrogen in blue; oxygen in red). (A), (E), (I) and (L) show the four hits bound in the orthosteric binding site of the antagonist-bound model of ECD-Asu-ACR-16. The front two subunits are highlighted (principal subunit, light pink; complementary subunit, yellow). The residues in the orthosteric binding site are labeled (principal side, pink; complementary side, orange) to show the location of the orthosteric binding site. (B), (F), (J) and (M) show the four hits bound in the agonist sub-pocket of the antagonist-bound model of ECD-Asu-ACR-16. The front two subunits are highlighted. The residues in the agonist sub-pocket are labeled (principal side, turquoise; complementary side, green) to show the location of the agonist sub-pocket. (C), (G) and (N) show the four hits bound in the intersubunit transmembrane site of the antagonist-bound model of TID-Asu-ACR-16. The front two subunits are highlighted. The residues in the intersubunit transmembrane site are labeled (principal side, pink; complementary side, orange) to show the location of the intersubunit transmembrane binding site. (D), (H), (K) and (O) show the four hits bound in the intrasubunit transmembrane site of the antagonist-bound model of TID-Asu-ACR-16. The residues in the intrasubunit transmembrane site are labeled (purple/blue) to show the location of the intersubunit transmembrane binding site. (For interpretation of the references to colour in this figure legend, the reader is referred to the web version of this article.)

were prepared, except for SB-277011-A where a stock solution of 10 mM was prepared due to the solubility; stock solutions were

frozen until required. Working solutions were then prepared by dilution on the day of the experiment.

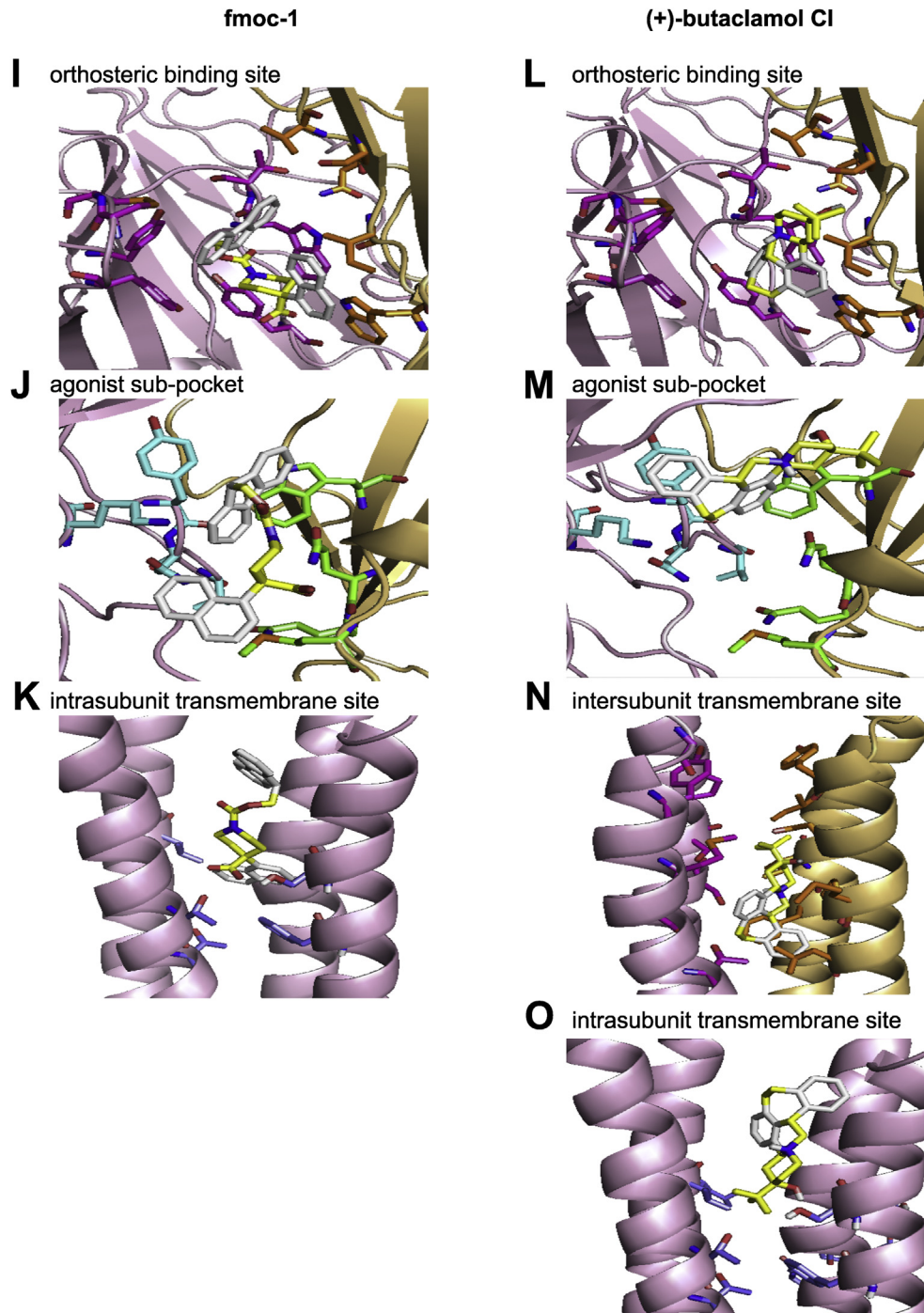


Fig. 3. (continued)

2.7. Pharmacological characterization of molecules selected by virtual screening

To characterize the four hits (Table 1) selected by our virtual screening, each drug was applied for 10 s to the oocytes expressing Asu-ACR-16 to test if the drugs were agonists. They were then tested as antagonists against ach.

To characterize the antagonistic properties of the four hits, the following protocol was used: a) 10 s of 100 μM ach alone; b) then 10 s of 100 μM ach + hit and then; c) 10 s of 100 μM ach alone. This test procedure was repeated with increasing concentrations of the

four hits (Fig. 4A–D), to determine the inhibitory dose–response relationships and IC_{50} by fitting Hill equations to the inhibitory dose–response curves using GraphPad Prism 5.0 (Graphpad Software Inc., CA, USA). As a further study of the antagonism, each of the four hits was applied before and during 10 s test applications of increasing concentrations of ach (Fig. S4).

2.8. Data analysis

The data from electrophysiological recordings were analyzed using Clampfit 9.2 (Molecular Devices, CA, and USA) and GraphPad

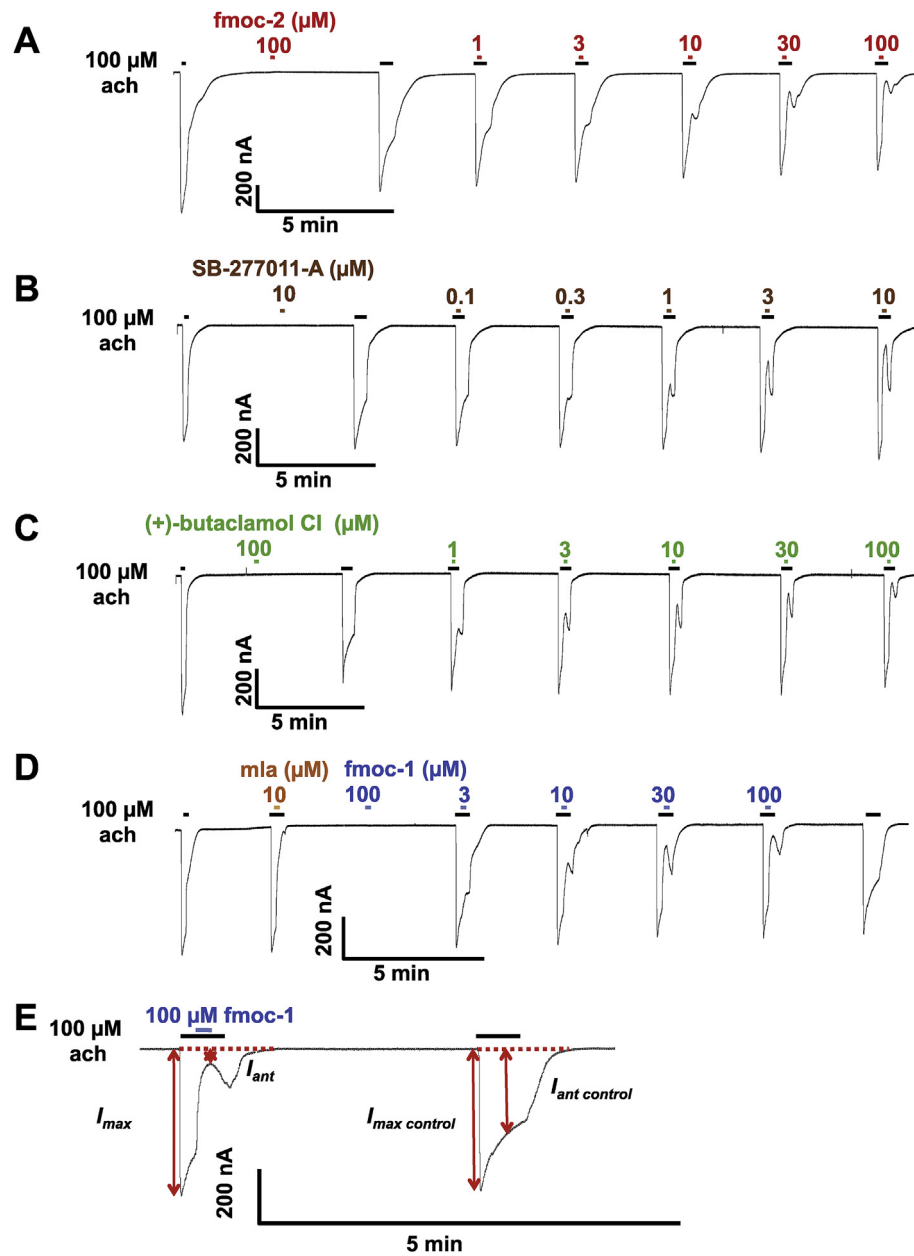


Fig. 4. Effects of four virtual screening hits on Asu-ACR-16 mediated ach responses. Sample traces for: (A) fmoc-2, (B) SB-277011, (C) (+)-butaclamol Cl, (D) fmoc-1 concentration-inhibition relationships on Asu-ACR-16. Mla in (D), which stands for methyllycaconitine citrate salt, was used as an antagonist control of Asu-ACR-16. All four hits did not induce the current response by themselves, while produced the concentration-dependent inhibition of ach current response. (E) is the magnified figure of part of (D) as an example to show the four parameters needed to measure the inhibition percentage. $I_{max\ control}$ was the peak current of the control 30 s application of 100 μM ach. I_{max} was the peak current of the 100 μM ach that preceded the 10 s co-application of ach and antagonist. I_{ant} was the minimal current during the co-application of 100 μM ach and antagonist. $I_{ant\ control}$ was the current at the same time point from the beginning of the 30 s application as I_{ant} during the control 30 s application of 100 μM ach.

Prism 5.0 (Graphpad Software Inc., CA, USA). In all recordings, the peak currents in response to applied drugs were measured, which were later normalized to the control 100 μM ach response, and expressed as mean \pm S.E.M. The mean % inhibition of currents elicited by 100 μM ach \pm S.E.M. was used to determine the inhibition percentage, which was quantified using the following equation:

$$\text{Inhibition}(\%) = \left(1 - \frac{I_{ant}}{\frac{I_{ant\ control}}{I_{max\ control}} \times I_{max}} \right) \times 100\%$$

where $I_{max\ control}$ was the peak current of the control 30 s application of 100 μM ach, I_{max} was the peak current of the 100 μM ach

that preceded the 10 s co-application of ach and antagonist. I_{ant} was the minimal current during the co-application of 100 μM ach and antagonist. $I_{ant\ control}$ was the current at the same point from the beginning of the 30 s application as I_{ant} during the control 30 s application of 100 μM ach (Fig. 4E). Concentration-response relationships or concentration-inhibition (%) relationships were analyzed by fitting data points into the Hill equation, with at least four replicates of each experiment set.

2.9. Drug treatment of *C. elegans*

The wild-type *C. elegans* strain N2 were obtained from the Caenorhabditis Genetics Center (University of Minnesota, MN,

Table 2
Binding affinities (kcal/mol) of the four hits and ach in the orthosteric binding sites of the three different bound models of ECD-Asu-ACR-16 and three allosteric binding sites of the antagonist-bound model of full-length Asu-ACR-16.

Hits	Binding affinities (kcal/mol)					
	Apo		Antagonist-bound		Transmembrane site	
	Orthosteric binding site	Orthosteric binding site	Orthosteric binding site	Agonist sub-pocket	Inter-subunit	Intra-subunit
fmoc-2	−10.4	−13.0	−10.2	−8.5	−11.4	−10.8
SB-277011-A	−9.8	−12.3	−9.2	−9.5	−10.8	−9.7
fmoc-1	−10.6	−12.3	−10.3	−8.9	NA	−11.0
(+)-butaclamol Cl	−9.5	−11.8	−8.2	−9.2	−10.8	−9.0
ach	−4.2	−4.3	−3.9	−4.0	−3.7	NA

USA). We grew *C. elegans* at 20 °C on nematode growth media (NGM, 3 g/l NaCl, 17 g/l agar, 2.5 g/l peptone, 1 mM CaCl₂, 5 mg/l cholesterol, 1 mM MgSO₄, 25 mM KPO₄ buffer) agar plates, seeded with *Escherichia coli* OP50 lawn under standard conditions (Brenner, 1974). Ten larvae at L4 stage with active thrashing movement (defined as “normal”) were transferred from NGM plates into M9 buffer (3 g/l KH₂PO₄, 6 g/l Na₂HPO₄, 5 g/l NaCl, 1 mM MgSO₄) in 24-wall plates for each treatment. We counted the number of worms with normal motility in M9 buffer with diluted drugs from the stock solutions (≤1% DMSO) at 0, 5, 10, 15 and 20 min. Five replicates were applied for each treatment. Motility between negative control (1% DMSO, final concentration) and drug treated worms were compared at each time point using student t-test.

3. Results

3.1. Sequence alignment of Asu-ACR-16 and template homologue proteins

The full-length protein sequence of Asu-ACR-16 (504 residues) was retrieved from the SwissProt database, of which the ECD-Asu-ACR-16 accounts for 234 residues. The first 25 residues of Asu-ACR-16 were excluded from alignment with the full length human nAChR $\alpha 7$ chimera (204 residues) because of the shorter length of the template protein sequence. The human $\alpha 7$ nAChR chimera shows 37.6% sequence identity and 72.9% sequence similarity with the ECD-Asu-ACR-16, based on the alignment generated by CLUSTALW (Fig. 1A, job ID: 65782ad6ad6d). The TID-Tma-nAChR subunit A shows 22.0% sequence identity and 45.4% sequence similarity with TID-Asu-ACR-16, aligned by CLUSTALW (Fig. 1B, job ID: 644888f4f30e). The residues involved in the putative orthosteric and the allosteric binding sites are highlighted in amino acids sequence of Asu-ACR-16.

3.2. Models of the Asu-ACR-16 pentamer

The model of the antagonist-bound form of the ECD-Asu-ACR-16 subunit starts from an N-terminal α helix followed by seven β strands that comprise an immunoglobulin fold. Loop A (Val114 – Ala122), loop B (Lys169 – Lys179), loop C (Phe213 – Pro220) from the principal subunit, and loop D (Ala78 – Ala83), loop E (Ile143 – Pro144), loop F (Gly185 – Met204) from the complementary subunit are involved in forming the orthosteric binding site. A disulphide bond between Cys152 and Cys166 contributes to the characteristic component of Cys-loop receptors. The C-terminal continues into the transmembrane domain (Fig. S1A).

The transmembrane domains of the Asu-ACR-16 model are made of four α -helices (M1, M2, M3 and M4). M1 links to the $\beta 7$ sheet of the extracellular domain and extends down into the membrane and is followed by the M2 and the M3 helices as the membrane-spanning portions. The MA cytoplasmic loop (helix

connects between M3 and M4. The region between M3 and MA is not modeled due to the poorly defined intracellular domain of the template structure. The C-terminal follows the M4 helix and faces toward the extracellular surface (Fig. S1B).

The pentameric model of Asu-ACR-16 has a five-fold symmetric around the channel pore. The average pairwise Root Mean Square Deviation (RMSD) fit of the C α coordinates of the antagonist-bound ECD-Asu-ACR-16 pentameric model and human $\alpha 7$ nAChR chimera pentamer (PDB code: 4HQP) was 0.9 Å, which indicates a strong structural conservation between the model and the template structures (Fig. S1C). The C α -RMSD between the TID-Asu-ACR-16 pentamer and the TID-Tma-AChR pentamer was 1.5 Å, which shows the TID fit is still good but not as good as the ECD fit. The membrane-spanning domains are arranged symmetrically. The M2 helix lines the channel pore, while M1, M3 and M4 do not contribute to the channel pore and are arranged peripherally (Fig. S1D).

Since no binding site data of Asu-ACR-16 is available to date, we used the published orthosteric binding site and allosteric binding sites in nAChRs or other Cys-loop receptors to predict the putative binding sites in Asu-ACR-16 (Galzi et al., 1991; Arias, 2000; Young et al., 2008; Hibbs and Gouaux, 2011; Spurny et al., 2015). The orthosteric binding site is at the interface between the principal site and the complementary site in two adjacent subunits of the ECD-Asu-ACR-16 pentamer (Fig. 2 S2A & S2B). The principal subunit (+) has vicinal cysteines (Cys216, Cys217) that contributes to the loop C of the binding site. The complementary subunit (−) does not use vicinal cysteines as part of the binding pocket and the residues are more variable when nAChRs are compared. The agonist sub-pocket, which we argue is a less significant allosteric binding site in ECD-Asu-ACR-16, is located right below the orthosteric binding site in the extracellular domain (Fig. 2 S2C & S2D). The vestibule pocket (Fig. S2E & S2F) and the top pocket (Fig. S2G & S2H) were not high affinity binding sites for the ligands and are not discussed further in this manuscript. The intersubunit allosteric binding sites in TID-Asu-ACR-16 are at the interface region between M2(+), M3(+), M1(−) and M2(−) (Fig. 2 S2I & S2J). The intrasubunit allosteric binding sites are at the center of the four transmembrane helices (M1, M2, M3 and M4) in each of the five subunits.

3.3. Binding properties of virtual screening hits

We carried out virtual screening of the ZINC ligand-database by using the three different bound forms of the ECD-Asu-ACR-16 models. Four molecules were selected as hits based on their high binding affinities and appropriate binding modes within the ligand-binding sites. The 9-fluorenylmethoxycarbonyl group (FMOC) was observed in twelve out of top forty hits ranked by binding affinities and exists in the two out of four hits, which suggests that FMOC could be necessary for the ligand recognition by the receptor. The FMOC group has a low predicted bioavailability due to the biphenyl scaffold, which limits aqueous solubility and

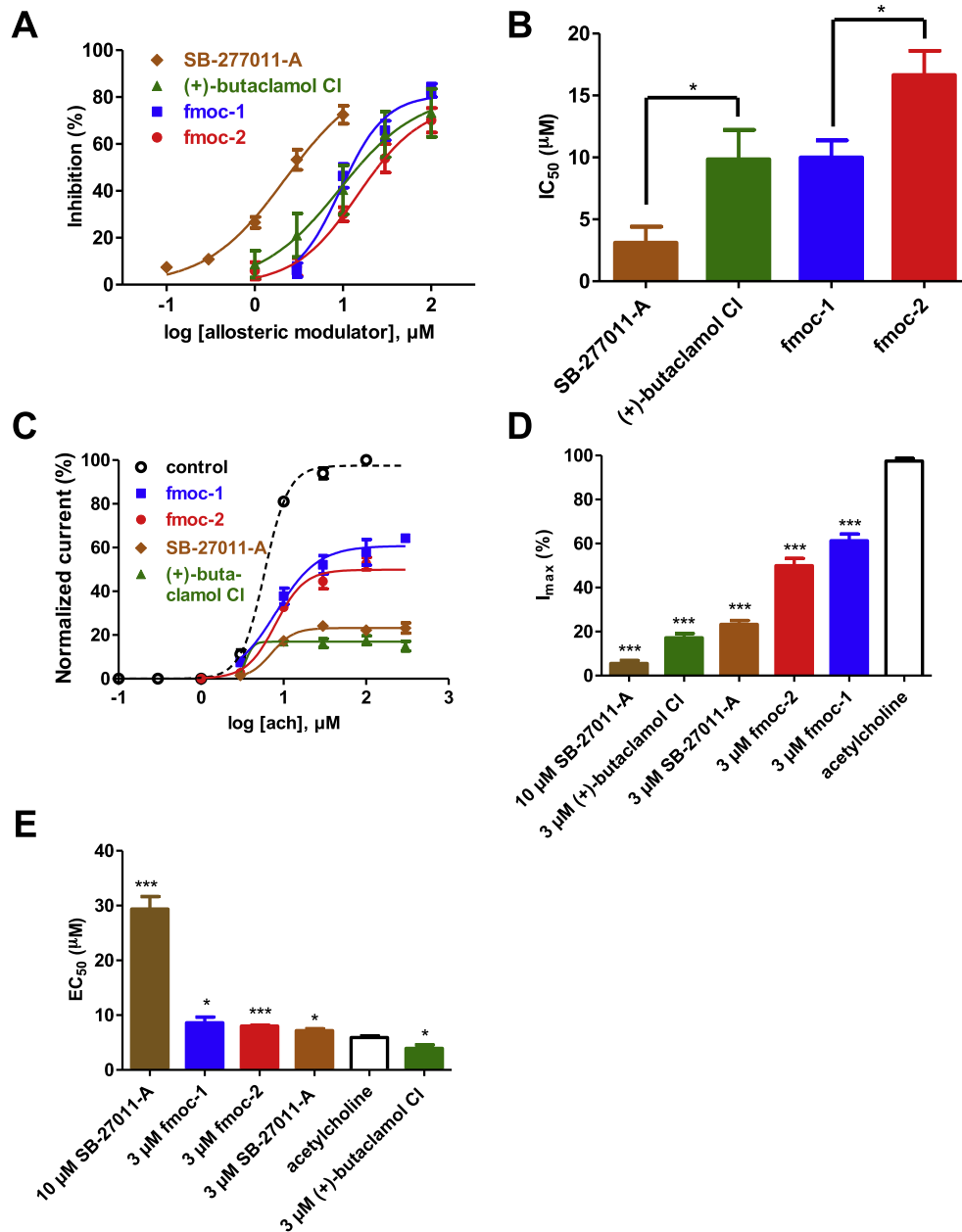


Fig. 5. (A) Effects of four virtual screening hits on Asu-ACR-16 mediated ach responses. Fmoc-2, fmoc-1, (+)-butaclamol Cl and SB-277011-A concentration-inhibition curves for Asu-ACR-16. Results were expressed as mean % inhibition of currents elicited by 100 μM ach ± S.E.M. (B) Bar chart representing the IC₅₀ (mean ± S.E.M., μM) of each plots in (A). The rank order series of inhibition based on IC₅₀ for four hits is: SB-277011-A (3.12 ± 1.29 μM, n = 4) < (+)-butaclamol Cl (9.85 ± 2.37 μM, n = 4) ≈ fmoc-1 (10.00 ± 1.38 μM, n = 4) < fmoc-2 (16.67 ± 1.95 μM, n = 4). * represents p < 0.05 (unpaired t-test). (C) Ach concentration-response plots for Asu-ACR-16 in the absence of hits as a control (ach) and in the continual presence of four hits identified in (A). Ach concentration-response curves for Asu-ACR-16 in the presence of 3 μM of four hits: fmoc-1, fmoc-2, SB-27011-A and (+)-butaclamol Cl. (D) Bar chart (mean ± S.E.M., %) representing the reduced maximum current response of ach concentration-response curves in (C). The series of reduced maximum response of each hits compared to that of ach by unpaired t-test is: 10 μM SB-27011-A (5.51 ± 1.38%, n = 4), 3 μM (+)-butaclamol Cl (17.22 ± 1.94%, n = 4), 3 μM SB-27011-A (23.25 ± 1.80%, n = 5), 3 μM fmoc-2 (49.92 ± 3.27%, n = 4), 3 μM fmoc-1 (61.25 ± 3.08%, n = 4) and ach (97.45 ± 1.19%, n = 4). * represents p < 0.05, ** represents p < 0.01, *** represents p < 0.001. All four hits significantly inhibited the maximum current response induced by ach. (E) Bar chart (mean ± S.E.M., μM) displaying the EC₅₀ of ach concentration-response curves in (C). The series of variable EC₅₀ of each hits compared to that of ach by unpaired t-test is: 10 μM SB-27011-A (29.40 ± 2.27 μM, n = 4), 3 μM fmoc-1 (8.01 ± 1.04 μM, n = 4), 3 μM fmoc-2 (8.01 ± 0.18 μM, n = 4), 3 μM SB-27011-A (7.17 ± 0.33 μM, n = 5), ach (5.92 ± 0.29 μM, n = 4) and 3 μM (+)-butaclamol Cl (3.94 ± 0.66 μM, n = 4). The EC₅₀ of all four hits obviously shift away from the control when applied.

may affect distribution to the *A. suum* parasite. Table 1 lists the physicochemical characteristics of four hits. They have relatively high molecular weights and are more hydrophobic compared to known Asu-ACR-16 agonists. However, they do follow the Lipinski's rule of five, which suggests that these molecules may be orally active (Lipinski et al., 2001; Lipinski, 2004).

The atomic structure predicts the partition-coefficients (XlogP) of the four hits to be between 4.27 and 6.04 (Table 1). The XlogPs suggest that the four hits are 10,000–1,000,000 times more concentrated in the lipophilic phase of the lipid bilayer than the aqueous phase of the extracellular domain (Cheng et al., 2007). The four hydrophobic hits are, therefore, more likely to bind into the

Table 3

Pharmacological profiles of the inhibitory effects of four hits on Asu-ACR-16 mediated ach responses. Results (mean \pm S.E.M.) were expressed as IC₅₀ (μ M), Hill slope (n_H), maximum inhibition (%) and the number of repeats (N) of each experiment.

Hits	IC ₅₀ (μ M)	n _H	Inhibitionmax (%)	N
fmoc-2	16.67 \pm 1.95	1.22 \pm 0.17	80.34 \pm 10.32	4
SB-277011-A	3.12 \pm 1.29	0.99 \pm 0.11	96.07 \pm 10.66	4
fmoc-1	10.00 \pm 1.38	1.97 \pm 0.37	82.49 \pm 4.74	4
(+)-butaclamol Cl	9.85 \pm 2.37	1.34 \pm 0.29	79.53 \pm 12.41	4

Table 4

Pharmacological profiles of EC₅₀ shifts and maximum current reductions of Asu-ACR-16 mediated ach responses in the presence and absence of four hits. Results (mean \pm S.E.M.) were expressed as EC₅₀ (μ M), Hill slope (n_H) and maximum response (%) and the number of repeats (N) of each experiment.

Hits	EC ₅₀ (μ M)	n _H	I _{max} (%)	N
control	5.92 \pm 0.29	3.05 \pm 0.07	97.45 \pm 1.19	4
3 μ M fmoc-2	8.01 \pm 0.18	2.54 \pm 0.18	49.92 \pm 3.27	5
1 μ M SB-277011-A	9.85 \pm 4.80	2.60 \pm 0.71	75.96 \pm 4.40	4
3 μ M SB-277011-A	7.17 \pm 0.33	3.37 \pm 0.28	23.25 \pm 1.80	5
10 μ M SB-277011-A	29.40 \pm 2.27	7.43 \pm 3.30	5.51 \pm 1.38	4
3 μ M fmoc-1	8.62 \pm 1.04	1.76 \pm 0.21	61.25 \pm 3.08	4
1 μ M (+)-butaclamol Cl	4.54 \pm 0.92	9.64 \pm 4.14	30.34 \pm 4.03	4
3 μ M (+)-butaclamol Cl	3.94 \pm 0.66	12.75 \pm 3.63	17.22 \pm 1.94	4

transmembrane allosteric binding pockets rather than to the extracellular ligand binding sites. The four hits which bind in the transmembrane allosteric binding pockets are therefore predicted to be allosteric modulators of the Asu-ACR-16 receptor that alter the activity of the agonists or competitive antagonists that bind to orthosteric binding site. SB-277011-A is known to be a potent and selective dopamine D₃ receptor antagonist with high oral availability (Stemp et al., 2000). (+)-butaclamol Cl is a non-selective dopamine receptor antagonist and a potent antipsychotic agent (Chrzanowski et al., 1985). No paper reporting on the activities of fmoc-2 and fmoc-1 has been published to date.

The four hits (Table 1) were tested for docking into the orthosteric binding sites of the three forms of ECD-Asu-ACR-16 models and the five allosteric binding pockets in the antagonist-bound form of full-length Asu-ACR-16 models. All four hits bound to the orthosteric binding sites of three ECD-Asu-ACR-16 models, but only bound to the three allosteric binding sites out of five: the intersubunit and intrasubunit transmembrane pockets and the agonist sub-pocket (Fig. 3) with high binding affinities.

In the intersubunit transmembrane site of TID-Asu-ACR-16 model, M243 (M1, (-)), L247 (M1, (-)) make hydrophobic interactions with naphthalene of fmoc-2. T312 (M3, (+)), S284 (M2, (+)) form hydrogen bonds with carboxylic acids of fmoc-2. F279 (M2, (-)), I282 (M2, (-)) and make hydrophobic contacts with fluorene of fmoc-2. F279 (M2, (-)), P244 (M1, (-)) make hydrophobic interactions with tetrahydroisoquinoline of SB-277011-A. N240 (M1, (-)) forms a hydrogen bond with carboxamide of SB-277011-A. P288 (M2, (+)) has hydrophobic interactions with quinoline of SB-277011-A. L247 (M1, (-)), F279 (M2, (-)) and makes hydrophobic contacts with dibenzocycloheptene of (+)-butaclamol Cl.

Ach, the natural agonist of Asu-ACR-16 was docked into the ligand binding sites of three forms of Asu-ACR-16 models for comparison. As expected, ach bound to the orthosteric binding site of the agonist-bound Asu-ACR-16 with an affinity (-4.3 kcal/mol), which was higher than the affinities at the other binding sites. The binding pose of ach docked in the orthosteric binding site of the agonist-bound Asu-ACR-16 model was in agreement with the binding pose of ach in the *L. stagnalis* AChBP cocrystal structure

(PDB code: 3WIP; Olsen et al., 2014b). The quaternary ammonium of ach faces the basal side of the binding cavity and make cation- π interaction with five aromatic residues from the Asu-ACR-16 ((+): Y89, W143, Y185, Y192; (-): W53), while the carbonyl oxygen of ach faces toward the apical side of the binding cavity. The binding affinities of the selected four compounds were higher than -8.0 kcal/mol in the three different bound forms of Asu-ACR-16, while the binding affinities of ach were lower than -4.5 kcal/mol in three states of Asu-ACR-16 (Table 2).

3.4. Pharmacological properties of virtual screening hits

We tested the effects of the putative allosteric modulators on Asu-ACR-16 receptors expressed in *Xenopus* oocyte using two-electrode voltage clamp to observe the currents that flow through Asu-ACR-16 receptors. Representative traces showing the inhibitory dose-response relationships are shown in Fig. 4. Their IC₅₀ (Fig. 5A and B) and maximum inhibition (Fig. S3) were determined as described in the methods (Table 3). The most potent antagonist among them was SB-277011-A, which had an IC₅₀ of 3.12 \pm 1.29 μ M and maximum inhibition effect of 96.07 \pm 10.66% (n = 4).

The ach concentration-response plots in the presence of 3 μ M of each putative allosteric modulator (Fig. S4 & Fig. 5C), show the reduced maximum current responses with little shift in EC₅₀ of ach (Fig. 5D and E & Table 4), and that the hits were non-competitive antagonists and negative allosteric modulators.

At 10 μ M, SB-277011-A, showed evidence of a mixed competitive and non-competitive antagonism (Fig. S5), characterized by a reduced maximum current response and a right-shift in the EC₅₀ of ach (Fig. 5D and E). Thus, 10 μ M SB-277011-A appears to act at more than one binding site which may include the orthosteric binding sites and additional allosteric binding sites.

3.5. SB-277011-A reversibly inhibits locomotion in *C. elegans*

We tested the effects of each allosteric modulator on the locomotion of *C. elegans* L4 larvae. The number of normal worms with thrashing-like movement dropped by 60% in 5 min after exposed to 30 μ M SB-277011-A (p < 0.01, n = 5, t-test). Paralysis-like movement was observed in the rest of the worms. Interestingly, the number of worms with motility that appeared normal recovered to 50% (p < 0.05, n = 5, t-test) in 10 min, 85% in 15 min (p > 0.05, n = 5, t-test) and returned to near negative control values after 20 min (Fig. S6). The recovery may relate to the desensitization properties of the ACR-16 receptor. The reversible inhibition of motility in worms was also observed in 100 μ M (+)-butaclamol Cl, but no significant difference between the number of normal treated worms and negative control was observed at any time point. No visual effects of 100 μ M fmoc-2 or 100 μ M fmoc-1 were found on the locomotion of worms.

4. Discussion

4.1. Asu-ACR-16 models

We have built up three-dimensional models of full-length structures of Asu-ACR-16 at the atomic level for the first time. We used homology modeling based on X-ray crystal structures of human α 7 nAChR chimeras and the electron microscopic structure of the *T. marmorata* nAChR as templates for different domains. The quality of our homology models are dependent on the sequence identity of the templates (human α 7 nAChR chimeras and *T. marmorata* nAChR) and the target sequence (Asu-ACR-16) and the resolutions of template structures (Hillisch et al., 2004; Cavasotto and Phatak, 2009). Our three ECD-Asu-ACR-16 models are likely

to be reliable for virtual screening because they have high sequence identities (37.6% identity and 72.9% similarity) with high resolution (<4 Å) templates. More errors might be expected in the TID-Asu-ACR-16 model, because of the missing loop between M3 and MA in the template structure which reduces sequence identity with the target protein. The missing loop does not include an allosteric binding site, so we can assume that the TID-Tma-nAChR structure is similar to the TID-Asu-ACR-16 structure (Bertrand et al., 2008). The overall secondary structures of our models are also consistent with published nAChRs structures (Finer-Moore and Stroud, 1984; Miyazawa et al., 2003; Unwin, 2005).

We developed the apo, the agonist-bound and the antagonist-bound models of the ECD-Asu-ACR-16 on the assumption that these three states of the Asu-ACR-16 receptor most closely represent the receptor conformations in the presence and absence of agonists or antagonists. To produce a realistic dynamic model would require more extensive work (Cavasotto and Orry, 2007; Spyrikis et al., 2011) and is beyond the scope of this study.

4.2. Virtual screening

Our structure-based virtual screening approach identified four novel and potent negative allosteric modulators of Asu-ACR-16, which were validated by our electrophysiological studies. The putative ligands were initially selected based on the virtual screening using the orthosteric binding site of the receptor. It was possible that these ligands could have been agonists or competitive antagonists that bind within the orthosteric binding site. In contrast, the pharmacological characterization of the four virtual screening hits shows that they behave as negative allosteric modulators and bind to allosteric sites. This outcome may be due to the hydrophobic properties of the four compounds that impedes their interactions with the orthosteric site in the extracellular domain of the receptor. The high lipid solubility of these compounds increases their concentration in the membrane lipid phase, in the region of the transmembrane allosteric sites.

The binding affinities calculated in the scoring function of AutoDock Vina software usually increase with the number of non-hydrogen atoms, which may be due to the neglect of desolvation in the scoring function (Shoichet et al., 1999; Kuntz et al., 1999; Park et al., 2006). This leads to a bias of virtual screening methods towards big molecules which are more hydrophobic, concentrated in the lipid bilayer, and less likely to interact with the binding sites in the extracellular domains (Hopkins et al., 2004). It is also pointed out that the simplified force fields used to estimate the binding free energies are unable to evaluate the conformational entropies and other contributions to the free energies (Cosconati et al., 2010). Thus, the success rate of identifying bioactive hits (44%) would be enhanced if we are able to include these additional parameters into a scoring function for virtual screening. Another approach, which we did not follow here, to enhance the success rate of identifying bio-active hits, is to use the known agonists or antagonists as scaffolds. This would facilitate the identification of low molecular-weight and more hydrophilic agonists or antagonists, and allow further study of the quantitative structure-activity relationships (Sun, 2008).

4.3. Four negative allosteric modulators of Asu-ACR-16

We evaluated the potency of inhibition for the four negative allosteric modulators in our electrophysiology studies on *Xenopus* oocytes: SB-277011-A (IC_{50} $3.12 \pm 1.29 \mu M$) < (+)-butaclamol Cl (IC_{50} $9.85 \pm 2.37 \mu M$) \approx fmoc-1 (IC_{50} $10.00 \pm 1.38 \mu M$) < fmoc-2 (IC_{50} $16.67 \pm 1.95 \mu M$). This rank of inhibition agrees with the level of effects of the four modulators in the motility of *C. elegans*. The

most potent modulator SB-277011-A was shown to decrease the motility of *C. elegans* larvae for a duration of about 10 min, yet less effective on adult *C. elegans*. Desensitization of the ACR-16 or other nAChRs in *C. elegans* body muscle may be a reason for the reduced effects of SB-277011-A on worms (Hernando et al., 2012). Treating the acr-16-null mutant of *C. elegans* with SB-277011-A can help us to investigate the mode of action of SB-277011-A on *C. elegans* as genetic models to understand SB-277011-A action on the parasitic nematode *A. suum* (Ward, 2015).

4.4. Allosteric binding sites may offer a better opportunity for drugs that can discriminate between the parasite Asu-ACR-16 and mammalian host $\alpha 7$ nAChR

Asu-ACR-16 shows 42.5% sequence identity and 71.2% sequence similarity with the human $\alpha 7$ nAChR (SwissProt ID: P36544) based on the alignment generated by CLUSTALW (Fig. S7, CLUSTALW job ID: cfd4f821eaf). The residues constituting the orthosteric binding site (pink and orange arrows in Fig. S7) are highly conserved between Asu-ACR-16 and human $\alpha 7$ nAChR, which shows 66.7% identity and 100% similarity (Fig. S8). In contrast, the residues of the four allosteric binding sites have much greater differences (variance) between the nematode parasite and the equivalent sites on the $\alpha 7$ receptor (identities: 62.5%, 45.5%, 66.7%, 62.5% and 40.0% and; similarities: 87.5%, 81.8%, 83.3, 93.8% and 100%). The sequence divergence in the allosteric binding sites between Asu-ACR-16 and host human $\alpha 7$ nAChR indicates that drugs targeted at these sites may be more selective than drugs targeted at orthosteric binding sites. Virtual screening specifically targeting the allosteric binding sites is predicted to offer a better opportunity for development of drugs with much greater receptor subtype selectivity (Nussinov and Tsai, 2013; Iturriaga-Vasquez et al., 2015).

4.5. Conclusion

We have developed a structure-based in silico screening approach to search for the bioactive hits that target at a parasitic nematode receptor. This approach allowed us to identify four negative allosteric modulators that were validated using our electrophysiological studies. These four compounds may be useful leads for anthelmintic drug discovery. We point out however, that we have not yet made the structural models for the host human $\alpha 7$ nAChR or other receptors, which would help to distinguish compounds that are active only on the nematode receptors, thereby reducing potential toxicity. It would also be desirable to perform virtual screening for toxicity on a range of host receptors, some structures of which have already been determined and others need to be modeled.

Statement of conflict of interest

None identified.

Acknowledgments

We would like to thank Tsung-Han Chou for the help and advice in modeling and docking. The research funding was by The Hatch Act, State of Iowa, and by NIH grants R01 AI047194 (to RJM) and AI114629 (to EWY) of the National Institute of Allergy and Infectious Diseases. The funding agencies had no role in the design, execution or publication of this study. The content is solely the responsibility of the authors and does not necessarily represent the official views of the National Institute of Allergy and Infectious Diseases.

Appendix A. Supplementary data

Supplementary data related to this article can be found at <http://dx.doi.org/10.1016/j.ijpddr.2016.02.001>.

References

- Abongwa, M., Buxton, S.K., Courtot, E., Charvet, C., Neveu, C., McCoy, C.J., Verma, S., Robertson, A.P., Martin, R.J., 2016. Pharmacological Profile of Asu-acr-16, a New Homomeric nAChR Widely Distributed in *Ascaris* Tissues (Under review).
- Adams, P.D., Afonine, P.V., Bunkoczi, G., Chen, V.B., Davis, I.W., Echols, N., Headd, J.J., Hung, L.W., Kapral, G.J., Grosse-Kunstleve, R.W., McCoy, A.J., Moriarty, N.W., Oeffner, R., Read, R.J., Richardson, D.C., Richardson, J.S., Terwilliger, T.C., Zwart, P.H., 2010. PHENIX: a comprehensive Python-based system for macromolecular structure solution. *Acta Crystallogr. Sect. D. Biol. Crystallogr.* 66, 213–221.
- Altschul, S.F., Madden, T.L., Schaffer, A.A., Zhang, J., Zhang, Z., Miller, W., Lipman, D.J., 1997. Gapped BLAST and PSI-BLAST: a new generation of protein database search programs. *Nucleic Acids Res.* 25, 3389–3402.
- Arias, H.R., 2000. Localization of agonist and competitive antagonist binding sites on nicotinic acetylcholine receptors. *Neurochem. Int.* 36, 595–645.
- Ballivet, M., Alliod, C., Bertrand, S., Bertrand, D., 1996. Nicotinic acetylcholine receptors in the nematode *Caenorhabditis elegans*. *J. Mol. Biol.* 258, 261–269.
- Berman, H.M., Westbrook, J., Feng, Z., Gilliland, G., Bhat, T.N., Weissig, H., Shindyalov, I.N., Bourne, P.E., 2000. The protein data bank. *Nucleic Acids Res.* 28, 235–242.
- Bertrand, D., Bertrand, S., Cassar, S., Gubbins, E., Li, J., Gopalakrishnan, M., 2008. Positive allosteric modulation of the alpha7 nicotinic acetylcholine receptor: ligand interactions with distinct binding sites and evidence for a prominent role of the M2–M3 segment. *Mol. Pharmacol.* 74, 1407–1416.
- Bethony, J., Brooker, S., Albonico, M., Geiger, S.M., Loukas, A., Diemert, D., Hotez, P.J., 2006. Soil-transmitted helminth infections: ascariasis, trichuriasis, and hookworm. *Lancet* 367, 1521–1532.
- Boulin, T., Fauvin, A., Charvet, C.L., Cortet, J., Cabaret, J., Bessereau, J.L., Neveu, C., 2011. Functional reconstitution of *Haemonchus contortus* acetylcholine receptors in *Xenopus* oocytes provides mechanistic insights into levamisole resistance. *Br. J. Pharmacol.* 164, 1421–1432.
- Boulin, T., Gielen, M., Richmond, J.E., Williams, D.C., Paoletti, P., Bessereau, J.L., 2008. Eight genes are required for functional reconstitution of the *Caenorhabditis elegans* levamisole-sensitive acetylcholine receptor. In: Proceedings of the National Academy of Sciences of the United States of America, 105, pp. 18590–18595.
- Brenner, S., 1974. The genetics of *Caenorhabditis elegans*. *Genetics* 77, 71–94.
- Buxton, S.K., Charvet, C.L., Neveu, C., Cabaret, J., Cortet, J., Peineau, N., Abongwa, M., Courtot, E., Robertson, A.P., Martin, R.J., 2014. Investigation of acetylcholine receptor diversity in a nematode parasite leads to characterization of tri-bendimidine- and derquantel-sensitive nAChRs. *PLoS Pathog.* 10, e1003870.
- Cavasotto, C.N., Orry, A.J., 2007. Ligand docking and structure-based virtual screening in drug discovery. *Curr. Top. Med. Chem.* 7, 1006–1014.
- Cavasotto, C.N., Phatak, S.S., 2009. Homology modeling in drug discovery: current trends and applications. *Drug Discov. Today* 14, 676–683.
- Celie, P.H., van Rossum-Fikkert, S.E., van Dijk, W.J., Brejc, K., Smit, A.B., Sixma, T.K., 2004. Nicotine and carbamylcholine binding to nicotinic acetylcholine receptors as studied in AChBP crystal structures. *Neuron* 41, 907–914.
- Changeux, J.-P., Edelman, S.J., 1998. Allosteric receptors after 30 years. *Neuron* 21, 959–980.
- Cheng, T., Zhao, Y., Li, X., Lin, F., Xu, Y., Zhang, X., Li, Y., Wang, R., Lai, L., 2007. Computation of octanol-water partition coefficients by guiding an additive model with knowledge. *J. Chem. Inf. Model.* 47, 2140–2148.
- Chrzanowski, F.A., McGrogan, B.A., Maryanoff, B.E., 1985. The pKa of butaclamol and the mode of butaclamol binding to central dopamine receptors. *J. Med. Chem.* 28, 399–400.
- Cosconati, S., Forli, S., Perryman, A.L., Harris, R., Goodsell, D.S., Olson, A.J., 2010. Virtual screening with autodock: theory and practice. *Expert Opin. Drug Discov.* 5, 597–607.
- Crompton, D.W., 2000. The public health importance of hookworm disease. *Parasitology* (121), S39–S50.
- de Silva, N.R., Brooker, S., Hotez, P.J., Montresor, A., Engels, D., Savioli, L., 2003. Soil-transmitted helminth infections: updating the global picture. *Trends Parasitol.* 19, 547–551.
- Devillers-Thiery, A., Giraudat, J., Bentaboulet, M., Changeux, J.P., 1983. Complete mRNA coding sequence of the acetylcholine binding alpha-subunit of Torpedo marmorata acetylcholine receptor: a model for the transmembrane organization of the polypeptide chain. In: Proceedings of the National Academy of Sciences of the United States of America, 80, pp. 2067–2071.
- Devillers-Thiery, A., Giraudat, J., Bentaboulet, M., Klarsfeld, A., Changeux, J.P., 1984. Molecular genetics of Torpedo marmorata acetylcholine receptor. *Adv. Exp. Med. Biol.* 181, 17–29.
- Emsley, P., Cowtan, K., 2004. Coot: model-building tools for molecular graphics. *Acta Crystallogr. Sect. D. Biol. Crystallogr.* 60, 2126–2132.
- Eswar, N., Webb, B., Marti-Renom, M.A., Madhusudhan, M.S., Eramian, D., Shen, M.Y., Pieper, U., Sali, A., 2007. Comparative Protein Structure Modeling Using MODELLER. *Current protocols in protein science/editorial board*, John E. Coligan... [et al.] (Chapter 2), Unit 2.9.
- Finer-Moore, J., Stroud, R.M., 1984. Amphipathic analysis and possible formation of the ion channel in an acetylcholine receptor. In: Proceedings of the National Academy of Sciences of the United States of America, 81, pp. 155–159.
- Galzi, J.-L., Bertrand, D., Devillers-Thiery, A., Revah, F., Bertrand, S., Changeux, J.-P., 1991. Functional significance of aromatic amino acids from three peptide loops of the $\alpha 7$ neuronal nicotinic receptor site investigated by site-directed mutagenesis. *FEBS Lett.* 294, 198–202.
- Halevi, S., Yassin, L., Eshel, M., Sala, F., Sala, S., Criado, M., Treinin, M., 2003. Conservation within the RIC-3 gene family. Effectors of mammalian nicotinic acetylcholine receptor expression. *J. Biol. Chem.* 278, 34411–34417.
- Hernando, G., Berge, I., Rayes, D., Bouzat, C., 2012. Contribution of subunits to *Caenorhabditis elegans* levamisole-sensitive nicotinic receptor function. *Mol. Pharmacol.* 82, 550–560.
- Hewitson, J.P., Maizels, R.M., 2014. Vaccination against helminth parasite infections. *Expert Rev. Vaccines* 13, 473–487.
- Hibbs, R.E., Gouaux, E., 2011. Principles of activation and permeation in an anion-selective Cys-loop receptor. *Nature* 474, 54–60.
- Hillisch, A., Pineda, L.F., Hilgenfeld, R., 2004. Utility of homology models in the drug discovery process. *Drug Discov. Today* 9, 659–669.
- Hopkins, A.L., Groom, C.R., Alex, A., 2004. Ligand efficiency: a useful metric for lead selection. *Drug Discov. Today* 9, 430–431.
- Hotez, P.J., Molyneux, D.H., Fenwick, A., Kumaresan, J., Sachs, S.E., Sachs, J.D., Savioli, L., 2007. Control of neglected tropical diseases. *N. Engl. J. Med.* 357, 1018–1027.
- Huang, S., Li, S.-X., Bren, N., Cheng, K., Gomoto, R., Chen, L., Sine, S.M., 2013. Complex between α -bungarotoxin and an $\alpha 7$ nicotinic receptor ligand-binding domain chimera. *Biochem. J.* 454, 303–310.
- Irwin, J.J., Sterling, T., Mysinger, M.M., Bolstad, E.S., Coleman, R.G., 2012. ZINC: a free tool to discover chemistry for biology. *J. Chem. Inf. Model.* 52, 1757–1768.
- Iturriaga-Vasquez, P., Alzate-Morales, J., Bermudez, I., Varas, R., Reyes-Parada, M., 2015. Multiple binding sites in the nicotinic acetylcholine receptors: an opportunity for polypharmacology. *Pharmacol. Res.* 101, 9–17.
- Keiser, J., Utzinger, J., 2008. Efficacy of current drugs against soil-transmitted helminth infections: systematic review and meta-analysis. *Jama* 299, 1937–1948.
- Krause, R.M., Buisson, B., Bertrand, S., Corringer, P.J., Galzi, J.L., Changeux, J.P., Bertrand, D., 1998. Ivermectin: a positive allosteric effector of the alpha7 neuronal nicotinic acetylcholine receptor. *Mol. Pharmacol.* 53, 283–294.
- Kuntz, I.D., Chen, K., Sharp, K.A., Kollman, P.A., 1999. The maximal affinity of ligands. In: Proceedings of the National Academy of Sciences of the United States of America, 96, pp. 9997–10002.
- Li, S.X., Huang, S., Bren, N., Noridomi, K., Dellisanti, C.D., Sine, S.M., Chen, L., 2011. Ligand-binding domain of an alpha7-nicotinic receptor chimera and its complex with agonist. *Nat. Neurosci.* 14, 1253–1259.
- Lipinski, C.A., 2004. Lead- and drug-like compounds: the rule-of-five revolution. *Drug Discov. Today Technol.* 1, 337–341.
- Lipinski, C.A., Lombardo, F., Dominy, B.W., Feeney, P.J., 2001. Experimental and computational approaches to estimate solubility and permeability in drug discovery and development settings. *Adv. Drug Deliv. Rev.* 46, 3–26.
- Martin, R., Robertson, A., 2010. Control of nematode parasites with agents acting on Neuro-Musculature Systems: lessons for Neuropeptide ligand discovery. In: Geary, T., Maule, A. (Eds.), *Neuropeptide Systems as Targets for Parasite and Pest Control*. Springer, US, pp. 138–154.
- Martin, R.J., Robertson, A.P., Buxton, S.K., Beech, R.N., Charvet, C.L., Neveu, C., 2012. Levamisole receptors: a second awakening. *Trends Parasitol.* 28, 289–296.
- Miyazawa, A., Fujiyoshi, Y., Unwin, N., 2003. Structure and gating mechanism of the acetylcholine receptor pore. *Nature* 423, 949–955.
- Moriarty, N.W., Grosse-Kunstleve, R.W., Adams, P.D., 2009. Electronic Ligand Builder and Optimization Workbench (eLBOW): a tool for ligand coordinate and restraint generation. *Acta Crystallogr. Sect. D. Biol. Crystallogr.* 65, 1074–1080.
- Morris, G.M., Goodsell, D.S., Halliday, R.S., Huey, R., Hart, W.E., Belew, R.K., Olson, A.J., 1998. Automated docking using a Lamarckian genetic algorithm and an empirical binding free energy function. *J. Comput. Chem.* 19, 1639–1662.
- Morris, G.M., Huey, R., Lindstrom, W., Sanner, M.F., Belew, R.K., Goodsell, D.S., Olson, A.J., 2009. AutoDock4 and AutoDockTools4: automated docking with selective receptor flexibility. *J. Comput. Chem.* 30, 2785–2791.
- Nussinov, R., Tsai, C.J., 2013. Allostery in disease and in drug discovery. *Cell* 153, 293–305.
- Olsen, J.A., Balle, T., Gajhede, M., Ahring, P.K., Kastrop, J.S., 2014a. Molecular recognition of the neurotransmitter acetylcholine by an acetylcholine binding protein reveals determinants of binding to nicotinic acetylcholine receptors. *PLoS One* 9, e91232.
- Olsen, J.A., Balle, T., Gajhede, M., Ahring, P.K., Kastrop, J.S., 2014b. Molecular recognition of the neurotransmitter acetylcholine by an acetylcholine binding protein reveals determinants of binding to nicotinic acetylcholine receptors. *PLoS One* 9.
- Pan, J., Chen, Q., Willenbring, D., Mowrey, D., Kong, X.P., Cohen, A., Divito, C.B., Xu, Y., Tang, P., 2012. Structure of the pentameric ligand-gated ion channel GLIC bound with anesthetic ketamine. *Structure* 20, 1463–1469.
- Park, H., Lee, J., Lee, S., 2006. Critical assessment of the automated AutoDock as a new docking tool for virtual screening. *Proteins* 65, 549–554.
- Peng, X., Katz, M., Gerzanich, V., Anand, R., Lindstrom, J., 1994. Human alpha 7 acetylcholine receptor: cloning of the alpha 7 subunit from the SH-SY5Y cell line and determination of pharmacological properties of native receptors and functional alpha 7 homomers expressed in *Xenopus* oocytes. *Mol. Pharmacol.*

- 45, 546–554.
- Polli, J.R., Dobbins, D.L., Kobet, R.A., Farwell, M.A., Zhang, B., Lee, M.H., Pan, X., 2015. Drug-dependent behaviors and nicotinic acetylcholine receptor expressions in *Caenorhabditis elegans* following chronic nicotine exposure. *Neurotoxicology* 47, 27–36.
- Qian, H., Martin, R.J., Robertson, A.P., 2006. Pharmacology of N-, L-, and B-subtypes of nematode nAChR resolved at the single-channel level in *Ascaris suum*. *FASEB J. official Publ. Fed. Am. Soc. Exp. Biol.* 20, 2606–2608.
- Raymond, V., Mongan, N.P., Sattelle, D.B., 2000. Anthelmintic actions on homomer-forming nicotinic acetylcholine receptor subunits: chicken $\alpha 7$ and ACR-16 from the nematode *Caenorhabditis elegans*. *Neuroscience* 101, 785–791.
- Rucktooa, P., Haseler, C.A., van Elk, R., Smit, A.B., Gallagher, T., Sixma, T.K., 2012. Structural characterization of binding mode of smoking cessation drugs to nicotinic acetylcholine receptors through study of ligand complexes with acetylcholine-binding protein. *J. Biol. Chem.* 287, 23283–23293.
- Rufener, L., Baur, R., Kaminsky, R., Maser, P., Sigel, E., 2010. Monepantel allosterically activates DEG-3/DES-2 channels of the gastrointestinal nematode *Haemonchus contortus*. *Mol. Pharmacol.* 78, 895–902.
- Rychlewski, L., Jaroszewski, L., Li, W., Godzik, A., 2000. Comparison of sequence profiles. Strategies for structural predictions using sequence information. *Protein Sci. A Publ. Protein Soc.* 9, 232–241.
- Shoichet, B.K., Leach, A.R., Kuntz, I.D., 1999. Ligand solvation in molecular docking. *Proteins* 34, 4–16.
- Spurny, R., Debaveye, S., Farinha, A., Veys, K., Vos, A.M., Gossas, T., Atack, J., Bertrand, S., Bertrand, D., Danielson, U.H., Tresadern, G., Ulens, C., 2015. Molecular blueprint of allosteric binding sites in a homologue of the agonist-binding domain of the $\alpha 7$ nicotinic acetylcholine receptor. In: *Proceedings of the National Academy of Sciences of the United States of America*, 112, pp. E2543–E2552.
- Spyrakakis, F., BidonChanal, A., Barril, X., Luque, F.J., 2011. Protein flexibility and ligand recognition: challenges for molecular modeling. *Curr. Top. Med. Chem.* 11, 192–210.
- Stemp, G., Ashmeade, T., Branch, C.L., Hadley, M.S., Hunter, A.J., Johnson, C.N., Nash, D.J., Thewlis, K.M., Vong, A.K.K., Austin, N.E., Jeffrey, P., Avenell, K.Y., Boyfield, I., Hagan, J.J., Middlemiss, D.N., Reavill, C., Riley, G.J., Routledge, C., Wood, M., 2000. Design and Synthesis of trans-N-[4-[2-(6-Cyano-1,2,3,4-tetrahydroisoquinolin-2-yl)ethyl]cyclohexyl]-4-quinolinecarboxamide (SB-277011): a potent and selective dopamine D3 receptor antagonist with high oral bioavailability and CNS penetration in the rat. *J. Med. Chem.* 43, 1878–1885.
- Sun, H., 2008. Pharmacophore-based virtual screening. *Curr. Med. Chem.* 15, 1018–1024.
- Thompson, J.D., Higgins, D.G., Gibson, T.J., 1994. CLUSTAL W: improving the sensitivity of progressive multiple sequence alignment through sequence weighting, position-specific gap penalties and weight matrix choice. *Nucleic Acids Res.* 22, 4673–4680.
- Trott, O., Olson, A.J., 2010. AutoDock Vina: improving the speed and accuracy of docking with a new scoring function, efficient optimization, and multi-threading. *J. Comput. Chem.* 31, 455–461.
- Unwin, N., 2005. Refined structure of the nicotinic acetylcholine receptor at 4 Å resolution. *J. Mol. Biol.* 346, 967–989.
- Wang, J., Czech, B., Crunk, A., Wallace, A., Mitreva, M., Hannon, G.J., Davis, R.E., 2011. Deep small RNA sequencing from the nematode *Ascaris* reveals conservation, functional diversification, and novel developmental profiles. *Genome Res.* 21, 1462–1477.
- Ward, J.D., 2015. Rendering the intractable more tractable: tools from *Caenorhabditis elegans* ripe for import into parasitic nematodes. *Genetics* 201, 1279–1294.
- Young, G.T., Zwart, R., Walker, A.S., Sher, E., Millar, N.S., 2008. Potentiation of $\alpha 7$ nicotinic acetylcholine receptors via an allosteric transmembrane site. In: *Proceedings of the National Academy of Sciences of the United States of America*, 105, pp. 14686–14691.